A Model-Based Investigation of Soil Moisture Predictability and Associated Climate Predictability

C. ADAM SCHLOSSER

Center for Ocean–Land–Atmosphere Studies, Calverton, Maryland

P. C. D. MILLY

U. S. Geological Survey, NOAA/Geophysical Fluid Dynamics Laboratory, Princeton, New Jersey

(Manuscript received 18 July 2001, in final form 14 March 2002)

ABSTRACT

Soil moisture predictability and the associated predictability of continental climate are explored as an initial-value problem, using a coupled land–atmosphere model with prescribed ocean surface temperatures. Ensemble simulations are designed to assess the extent to which initial soil moisture fields explain variance of future predictands (soil moisture, near-surface air temperature, and precipitation). For soil moisture, the decrease of explained variance with lead time can be characterized as a first-order decay process, and a predictability timescale is introduced as the lead time at which this decay reaches e^{-1}. The predictability timescale ranges from about 2 weeks or less (in midlatitudes during summer, and in the Tropics and subtropics) to 2–6 months (in mid- to high latitudes for simulations that start in late fall and early winter). The predictability timescale of the modeled soil moisture is directly related to the soil moisture's autocorrelation timescale. The degree of translation of soil moisture predictability to predictability of any atmospheric variable can be characterized by the ratio of the fraction of explained variance of the atmospheric variable to the fraction of explained soil moisture variance. By this measure, regions with the highest associated predictability of 30-day-mean near-surface air temperature (ratio greater than 0.5) are, generally speaking, coincident with regions and seasons of the smallest soil moisture predictability timescales. High associated temperature predictability is found where strong variability of soil moisture stress on evapotranspiration and abundant net radiation at the continental surface coincide. The associated predictability of 30-day-mean precipitation, in contrast, is very low.

1. Introduction

Since the pioneering work on atmospheric predictability (Lorenz 1965; Charney et al. 1966; Smagorinsky 1969), a wealth of numerical and observational studies have aimed to identify mechanisms of forced variability and, hence, sources of potential predictability for a climate system that is inherently chaotic. At the forefront of this research, studies have demonstrated that knowledge of slowly varying sea surface temperatures (SSTs) can enhance our ability to provide skillful monthly-to-seasonal atmospheric predictions (e.g., Lau 1990; Stern and Miyakoda 1995), and that the strongest interannual modes of SST variability, such as those associated with the El Niño–Southern Oscillation, are found to be skillfully predictable out to a 1-yr lead time (e.g., Shukla 1998). Additionally, a growing body of evidence indicates that slowly varying land surface conditions, in particular anomalies of continental water storage, have a discernible influence on climate variability. The theoretical and observational basis of the potential role of surface–atmosphere interactions on climate anomalies includes work as early as that of Namias (1963), and as recent, for example, as that of Durre et al. (2000). Within the past two decades, numerical experimentation has allowed a more explicit examination of the impact of interactive continental water balance on simulated atmospheric variability (e.g., Walker and Rowntree 1977; Yeh et al. 1984; Gordon and Hunt 1987; Delworth and Manabe 1988; Koster and Suarez 1996, to name a few). In these studies, the impact of modeled soil moisture variability and persistence on simulated near-surface atmospheric and precipitation variability is demonstrated. In addition, the potential for soil moisture initialization to aid in the accurate simulation of extreme climate events, such as droughts (e.g., Fennessy and Shukla 1999; Atlas et al. 1993; Namias 1991), has been shown. Overall, studies such as these demonstrate the impact that soil moisture anomalies can have on subsequent atmospheric variability and the persistence of extreme climate anomalies.

Remote sensing, models, and data assimilation can

Corresponding authors address: C. Adam Schlosser, NASA Goddard Space Flight Center, Code 974, Greenbelt, MD 20771.
E-mail: adam@hsb.gsfc.nasa.gov

produce estimates of large-scale (i.e., continental to global) fields of soil moisture (e.g., Houser et al. 1998; Walker and Houser 2001) potentially suitable for initialization of climate prediction models. However, it remains uncertain how useful such estimates would be for operational climate predictions, as most sensitivity studies have focused on extreme climatic events (e.g., Oglesby 1991; Atlas et al. 1993). Observational evidence (e.g., Huang and van den Dool 1993) supports the potential role of soil moisture information as an operational predictor for continental temperature fluctuations, and modeling (e.g., Dirmeyer 1999; Koster et al. 2000) shows that soil moisture information also has the potential to improve seasonal precipitation predictions under certain environmental conditions. Nevertheless, two questions arise with regard to soil moisture initialization in climate forecasts. First, how can the information be applied consistently with the definition, framework, and climatology of soil moisture in the forecast model? Second, given an optimal application of perfect soil moisture information, what is the ultimate increase in predictive skill that we can gain from knowing the initial and subsequently predicted soil moisture for climate forecasts? The first question primarily addresses the operational pitfalls that may arise from systematic biases between a coupled model and nature (e.g., Dirmeyer 1995; Mitchell et al. 1999). The second question focuses more on the fundamental limits of predictability of the climate system. Moreover, insights on the latter question might serve as a useful scientific guide toward efficiency in operational land-data assimilation products. Therefore, efforts should be made, through numerical experiments with a variety of climate models, to explicitly address the potential benefits of initial soil moisture information on climate predictability and operational climate prediction.

Herein, we explore the nature of soil moisture predictability and the associated climate predictability for a particular coupled land–atmosphere model using hypothetically perfect information on initial soil moisture. We conduct sets of ensemble simulations using a general circulation model (GCM) of the atmosphere coupled to an interactive land model that represents the water and energy balances of the continental surface. In the next section, we describe the coupled land–atmosphere GCM used for this study, the ensemble-simulation design, and the measure of predictability developed for this analysis. In section 3 we present the results of the GCM ensemble simulations. In addition, a discussion of the factors controlling soil moisture and its associated atmospheric predictability is presented. Concluding remarks are given in section 4.

2. Ensemble simulations

a. Model

Numerical experiments were conducted using the Geophysical Fluid Dynamics Laboratory (GFDL) climate model, which includes an atmospheric GCM (AGCM) coupled to a simple water- and energy-balance model of the continents [similar to that used in Milly and Dunne (1994)]. At the ocean–atmosphere interface, SSTs were prescribed to follow observed geographic and seasonal patterns, with no interannual variability. The GCM contains a dynamical core that solves the equations of motion through the use of spherical harmonics with a rhomboidal-15 (R15) wavenumber truncation in the horizontal and nine levels vertically. Grid-based (including land) computations are performed on a 7.5° longitude by 4.5° latitude grid. Daily-average solar forcing is specified. Clouds are predicted using a simple relative humidity criterion. Precipitation is calculated so as to prevent supersaturation of the air by water vapor. Vertical convection is treated by moist-convective adjustment of the atmosphere. This GCM has been shown by Delworth and Manabe (1988) to simulate the geographical distribution of seasonally (i.e., December–February and June–August) averaged precipitation and annually averaged runoff reasonably well against available observations. Moreover, the zonally averaged spectra of rainfall (plus snowfall) have a slightly red-noise characteristic. However, shortcomings do exist in the model and will be addressed with regard to the findings of this particular study in the concluding section.

The land parameterization is that described by Manabe (1969). Soil moisture is tracked in a single store, representing the plant-available water in the plant root zone. Soil moisture is depleted only by evaporation; runoff occurs only when storage capacity is exceeded as a result of infiltration of rainfall and snowmelt. The soil moisture (w) balance equation is

$$\frac{dw}{dt} = P - \beta E_p - R, \tag{1}$$

where

$$\beta = \min\left[\frac{w}{0.75w_0}, 1\right],$$

in which w_0 is the soil moisture capacity (0.15 m global constant), P is the sum of rainfall and snowmelt, E_p is the potential evaporation rate, and R is runoff, which occurs as needed to prevent soil moisture from exceeding the capacity. Snowpack is tracked as a separate water store. The land has no heat capacity, other than that associated with latent heat of fusion of snow. Figure 1 shows the representation of the continents by the model grid. Also denoted are six selected pairs of adjacent grid cells for which results are highlighted in this paper.

b. Experimental design

Within the climate model, the full state of the climate system at any time is described by global, two- and three-dimensional distributions of several ''prognostic''

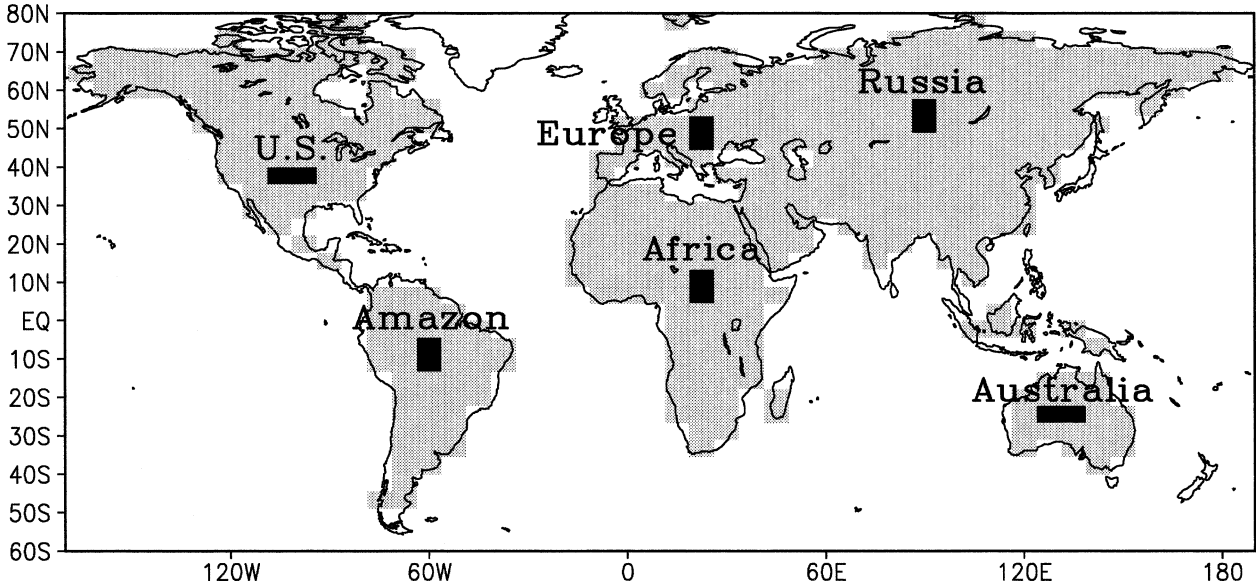

FIG. 1. Map showing locations and identifiers of adjoining grid-cell pairs for which detailed results are presented in other figures. Each shaded rectangle represents two cells having either the same latitude (United States, Australia) or longitude (all others).

variables. Soil moisture is one of these variables. For brevity, the remaining prognostic variables are herein collectively termed the ''atmospheric state'' of the model, although they include snowpack depth.

The ensemble simulations are designed to provide information on the extent to which the soil moisture field at the time of initialization predicts, on a seasonal timescale, later anomalies of soil moisture and atmospheric variables. For every month of the year (starting on the first day of the month), 80 1-yr simulations were run, using all combinations of 8 initial soil moisture fields and 10 initial atmospheric states. The soil moisture fields and atmospheric states were randomly saved from the corresponding time of year within 18 distinct years chosen from a 200-yr climatological run of the same climate model.

c. Measure of predictability

To characterize predictability, we shall introduce a measure of the proportion of any predictand's variability that can be explained by the initial soil moisture distribution. Each set of simulations using a common initial soil moisture field is termed an ensemble. We denote the ith ensemble mean of any predictand, f, by, $\overline{f}_i$,

$$\overline{f}_i = \frac{1}{N}\sum_{j=1}^{N} f_{ij}, \tag{2}$$

in which f_{ij} is the value of the predictand in the jth member of the ith ensemble, and N (=10, here) is the number of members in each ensemble. We define an intraensemble variance, S_A^2, of f by pooling results from all M (=8, here) ensembles,

$$S_A^2 = \frac{1}{MN}\sum_{i=1}^{M}\sum_{j=1}^{N}(f_{ij} - \overline{f}_i)^2. \tag{3}$$

Strictly speaking, this statistic and other quantities introduced below are neither variances nor unbiased estimators of variances, but the ''variance'' terminology is conveniently descriptive and will be used herein. Essentially, S_A^2 describes the spread of f within an ensemble, averaged over all ensembles. As a measure of the total variance of f, we introduce the quantity S_T^2, defined by

$$S_T^2 = \frac{1}{MN}\sum_{i=1}^{M}\sum_{j=1}^{N}(f_{ij} - \overline{f})^2, \tag{4}$$

in which $\overline{f}$ is the mean over all members of all ensembles,

$$\overline{f} = \frac{1}{M}\sum_{i=1}^{M}\overline{f}_i. \tag{5}$$

It can be shown that these two measures of variability differ by a measure of the variability across ensembles, which we shall call the interensemble variance, S_R^2, given by

$$S_T^2 - S_A^2 = S_R^2 = \frac{1}{M}\sum_{i=1}^{M}(\overline{f}_i - \overline{f})^2. \tag{6}$$

For our measure of predictability, we form the ratio of the interensemble variance to the total variance, and we call it the ''relative interensemble variance of f,'' R_f, given by

$$R_f = \frac{S_R^2}{S_T^2}. \tag{7}$$

Note that f and R_f can be defined for any predicted variable (e.g., soil moisture or atmospheric variable) or for any time or area average thereof. For any f selected for analysis, R_f will be a function of ''lead time'' (defined herein as the time since initialization).

How should we expect R_f to vary with lead time? When f is soil moisture (i.e., $R_f \equiv R_w$), all members of a given ensemble initially have the same value, by design, so R_w is initially equal to unity. As lead time advances, intraensemble differences in soil moisture will arise (due to initially different atmospheric states) and grow, causing a decrease in R_w. Sufficiently far into the future, assuming transitivity of the land–atmosphere system, separate members of an ensemble can be expected to ''lose the memory'' of the initial soil moisture. At such lead time, it can be shown that

$$E[S_T^2] \rightarrow \frac{MN - 1}{MN} S^2, \tag{8}$$

in which S^2 is the variance (in its conventional form) of f in the model. It can also be shown, for large lead time, that

$$E[S_A^2] \rightarrow \frac{N - 1}{N} S^2. \tag{9}$$

To a first approximation, it then follows that for any f

$$R_f \rightarrow R_\infty = \frac{M - 1}{MN - 1} = 0.089$$

(for our choice of M and N). (10)

The timescale of the decay of R_w from unity to this long lead-time value is a measure of the predictability of soil moisture.

For any atmospheric variable a, R_a is equal to zero at the start of the simulation period, because all initial atmospheric $\overline{f}_i$ are identical by the experimental design. At large lead time, R_a will approach the same asymptotic value found for soil moisture. Between these two endpoints, the behavior of R_a will depend on the extent to which the atmospheric variable is affected by soil moisture. If the atmospheric variable is not sensitive to soil moisture, then R_a can be expected to rise monotonically to its large lead-time value. If, however, soil moisture has a significant influence on the atmospheric variable, then R_a will initially rise with lead time to a peak higher than the large lead-time value, to which it will subsequently decline asymptotically. The timescale of the initial rise is determined by the response rate of the atmosphere to the underlying land, which we assume to be faster than the decay rate of R_w to R_∞. The apex of the rise should also be proportional to the sensitivity of the atmospheric variable to soil moisture. Furthermore, the timescale of the large lead-time decay of R_a (toward R_∞) is expected to follow that for soil moisture.

3. Predictability results

a. Soil moisture predictability

Gridpoint samples of R_w time series based on daily (end of day) soil moisture are shown in Fig. 2, using results from the simulations initialized in June. The time series have the characteristics predicted in the previous section: they start at unity and decay over lead time to a value that fluctuates around the expected asymptotic value. The decay is not regular but can be viewed as the sum of a smoothly decaying function of lead time and a random variation. The rate of decay, or characteristic timescale of the underlying smooth function, varies from one grid point to the next. In all presented cases, the decay to the asymptotic value is realized by a lead time of 3 months, but in some cases the decay is much faster. The size of the fluctuations at large lead time provides a simple index against which the significance of early-time predictability can be subjectively assessed.

To characterize the temporal behavior of R_w, we have fitted (via least squares) an exponential decay curve to each R_w as a function of lead time, t, given by

$$R_w(t) = (1 - R_\infty)e^{-t/\tau_W} + R_\infty, \tag{11}$$

in which R_∞ is the known long lead-time expectation for R_f [given by Eq. (10)], and τ_w is a characteristic timescale of soil moisture predictability (i.e., the e-folding timescale of the fitted exponential). Continuous lines in Fig. 2 show fits of Eq. (11) to the data, and Fig. 3 (top) shows the superposition of the $R_w(t)$ data from Fig. 2, using a normalized abscissa in time. The exponential function captures the essence of the underlying temporal decay of $R_w(t)$.

Also shown in Fig. 3 (bottom), for the same sample grid points, are histories of R_w based on 30-day mean soil moisture. These are constructed by taking $f(t)$ to be the 30-day running-mean value (in this case, soil moisture) centered around t, and then calculating R_f as given by Eqs. (2)–(7). The resultant quantity is hereafter referred to as ''30-day R_f,'' for any given f. The effects of using 30-day means instead of daily values are smoothing of the 30-day $R_w(t)$ curves and slight lengthening of the characteristic timescales. The analysis of soil-moisture predictability and atmospheric response that follows will be based on the 30-day R results.

The parameter τ_w is used to characterize the spatial and temporal pattern of soil moisture predictability. The time series for 30-day R_w at all land grid points and all initialization dates were computed and fitted to the exponential-decay model, and, hereafter, the timescale obtained from this calculation will be referred to as ''30-day τ_w.'' Figure 4 shows how the zonal mean values of the estimated 30-day τ_w depend on month of initialization and latitude. Values of 30-day τ_w range from less than a week in the Tropics to several months for the ensembles started during high-latitude fall and winter. Summer values of 30-day τ_w in the middle and high

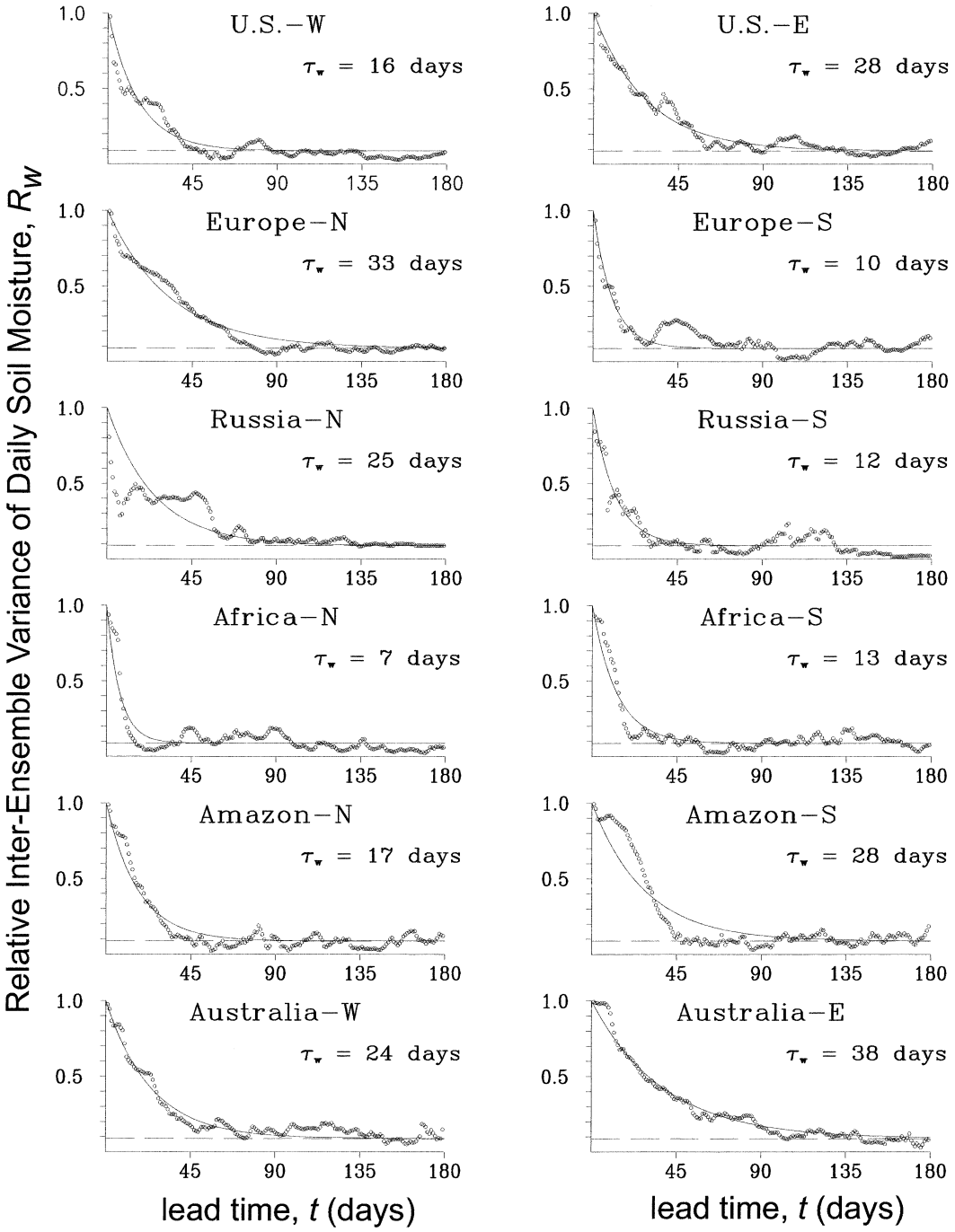

FIG. 2. Relative interensemble variance of daily soil moisture, R_w, for the selected grid-cell pairs (of Fig. 1), as a function of lead time, t (days). Each cell within a pair is denoted by its east/west (E/W) or north/south (N/S) position with respect to its counterpart. Results shown are from the simulations starting in June. Also shown are fitted exponential functions (solid curves) associated with τ_w, and theoretical value of R_∞ (dashed horizontal lines).

latitudes are typically in the range of 2–4 weeks. Most of the tropical and subtropical regions show relatively little seasonal variation and have relatively small 30-day τ_w values of approximately 1–2 weeks. The zone of minimum 30-day τ_w migrates from the northern Tropics during Northern Hemisphere summer to the southern Tropics during northern winter. The long timescales seen in the mid- and high-latitude winter initializations are, in part, contributed by snow cover, which decouples the soil moisture from the atmosphere in the GFDL GCM; that is, precipitation is not allowed into, nor evaporation from, the soil column (and recall there is no gravitational

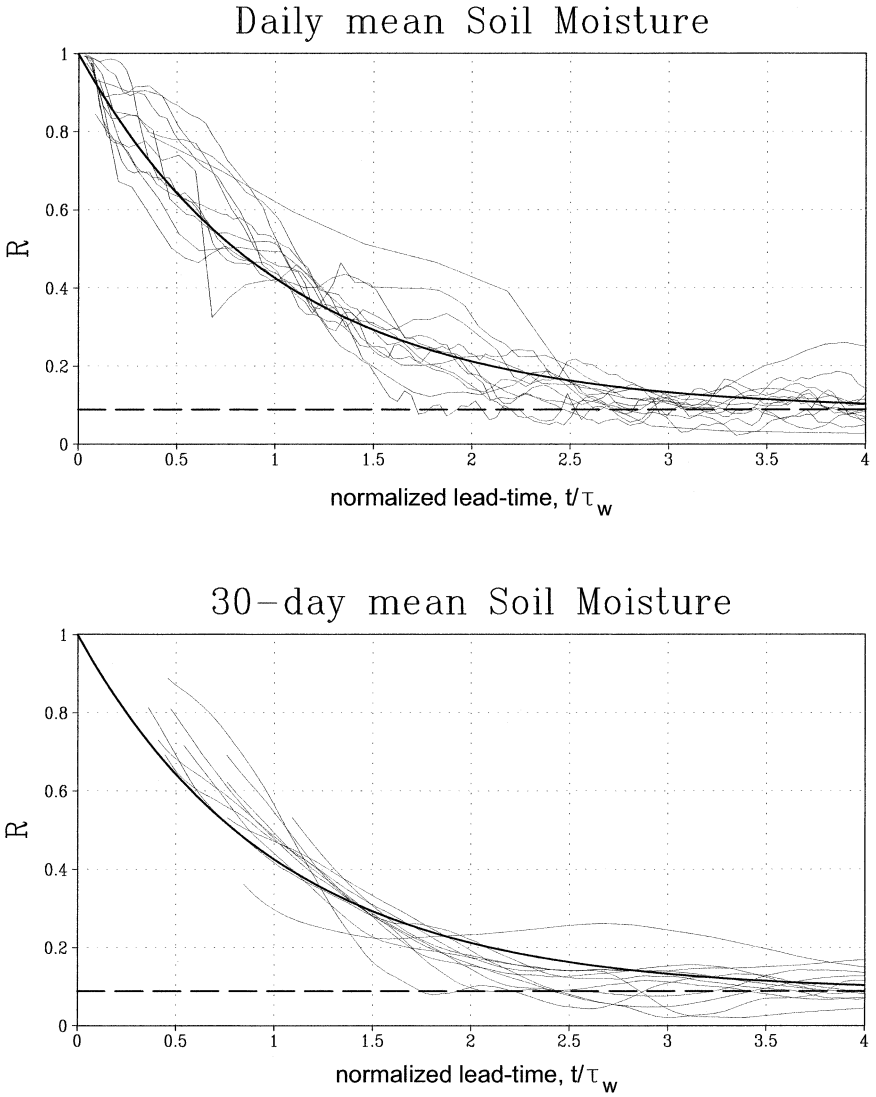

FIG. 3. Relative interensemble variance of (top) daily soil moisture, R_w and (bottom) 30-day mean soil moisture, 30-day R_w, for the selected grid cells of Fig. 1, as functions of normalized forecast lead time, t/τ_w. Distinct values of τ_w were determined separately for the daily and 30-day results. Results are from the ensemble simulations starting in June. Also shown is the exponential function (heavy solid curve) described by Eq. (11) and the theoretical value of R_∞ (dashed horizontal line).

drainage in the GFDL bucket formulation). Other controls of soil moisture predictability are addressed in section 4.

Figure 5 shows the global distribution of 30-day τ_w for June and December initializations. Because these are based on results from individual grid points, a significant amount of random noise is present in these results. Nevertheless, Fig. 5 suggests that global patterns of predictability depart in some regions from what would be predicted by the zonal-mean patterns already discussed in connection with Fig. 4. In particular, December 30-day τ_w are somewhat greater than the zonal average in central North America and in Asia, and less than the average in Europe and coastal North America.

b. Associated predictability of near-surface air temperature

Having reviewed the results for soil moisture predictability, we now examine the resultant predictability of near-surface air temperature (T) and precipitation (P). Sample $R_T(t)$ data, for daily T, are shown in Fig. 6. For some grid points (in particular the Amazon-S and U.S. points), the initial rise of R_T from zero at initial time is apparent; for others, the rise is so rapid as to be almost undetectable. At large lead time, R_T fluctuates randomly around the expected asymptotic value. At most grid points, the initial growth from zero leads into an intermediate lead-time regime when R_T tends to exceed the

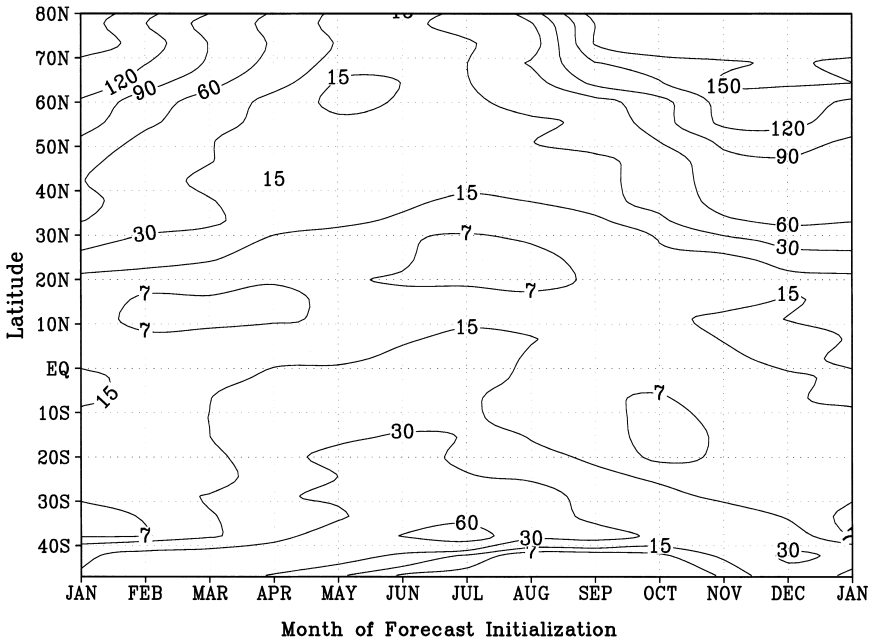

FIG. 4. Zonal-mean values (days; land only) of 30-day τ_w (as defined in the text), as a function of initialization date of the ensemble simulations and latitude.

asymptotic value. Accordingly, we can infer a certain degree of T predictability resulting from soil moisture predictability.

For those grid points in Fig. 6 with a significant initial rise of R_T above its asymptotic value, the timescale of its decay appears to be on the order of that of soil moisture predictability. Under our assumption that the atmospheric response time is small compared to 30-day τ_w (section 2c), it is reasonable to expect that R of atmospheric variables will decay to R_∞ on the same timescale as that of soil moisture. As seen in Fig. 6, R_T is generally less than R_w for a given lead time (even after its initial spinup from zero), indicating that a given level of soil moisture predictability does not translate fully to a corresponding level of T predictability.

It is reasonable to expect that time averages (low-frequency variations) of atmospheric variables will be more predictable than daily values (high-frequency variations), given that τ_w is typically on the order of weeks. For this reason, our analysis will focus henceforth on 30-day R_T (and R_P). Figure 7 shows 30-day R_T at our sample grid points. In comparison with Fig. 6 for daily values, the 30-day R_T values tend to be significantly larger at the intermediate time when predictability is apparent. In many cases, 30-day R_T is nearly equal in magnitude to the fitted 30-day R_w for a given lead time. Moreover, the expected proportional decay of R_T to R_w at long lead times is much more apparent for the 30-day means as compared to the daily plots (Fig. 6). The spinup period of 30-day R_T is largely absent, due to the time averaging and that 30-day R_T is undefined during the first 15 days of the simulation. At long lead times, 30-day R_T fluctuates around the predicted asymptotic value but with considerably greater temporal persistence than for daily R_T. A sensitivity test was performed for the simulations initialized on 1 June in which the number of ensembles, M, was increased from 8 to 16. The results showed considerable reduction in the long lead-time fluctuations while preserving the early lead-time peaks of 30-day R_T. This would suggest that the early lead-time peaks seen for our set of simulations where $M = 8$ can be viewed as robust.

To escape the apparent noise in gridpoint 30-day R_T, we display in Fig. 8 the zonal-mean values of 30-day R_T. Predictability of 30-day mean T is apparent at almost all latitudes, the only exceptions being north of 60°N and south of 30°S. For comparison, the corresponding 30-day R_w are shown. From 60°N to 10°S, zonal 30-day R_w and 30-day R_T converge within several weeks of initialization and decay together thereafter. During the initial phase before convergence, 30-day R_w exceeds 30-day R_T, and we associate this with the initial spinup of the atmospheric state. The near-coincidence of the zonal 30-day R curves after the time of convergence implies full translation of soil moisture predictability to air temperature predictability, suggesting near-total control of near-surface air temperature anomalies by soil moisture anomalies at the 30-day timescale. This correspondence breaks down in the Southern (winter) Hemisphere, between 10° and 40°S, as the predictability of near-surface air temperature decreases progressively to zero, despite

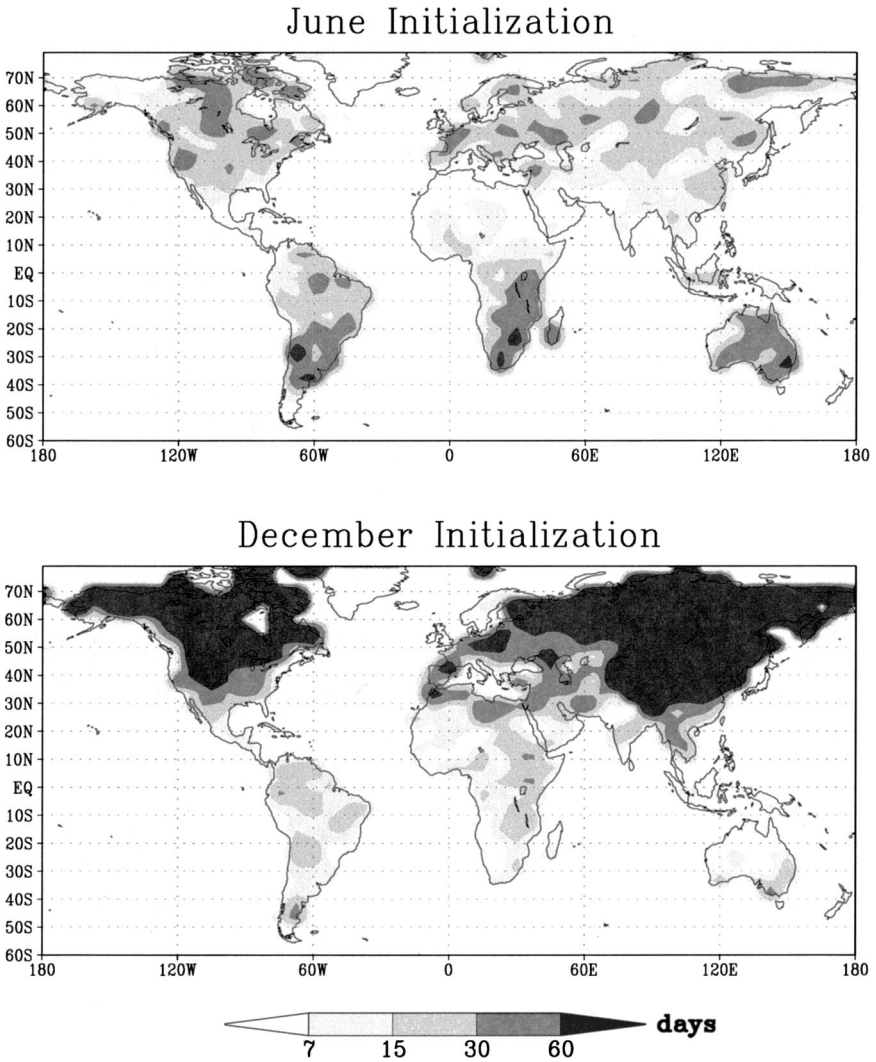

FIG. 5. Global distribution of 30-day τ_w for ensemble simulations starting (top) 1 Jun and (bottom) 1 Dec.

increasing soil moisture predictability (i.e., larger values of 30-day τ_w).

As Fig. 8 shows, the relation of 30-day R_w to atmospheric-variable 30-day R can provide a measure of atmospheric response to a given level of soil moisture predictability. To formalize this, we introduce the ''associated predictability ratio'' for any atmospheric variable, a, as

$$A_a = \frac{R_a(t) - R_\infty}{R_w(t) - R_\infty}. \quad (12)$$

Note that A cannot be independent of time until after the initial atmospheric spinup, and even then only as an approximation. To allow for the spinup period, we refine this relation to

$$R_a(t) - R_\infty = A_a[1 - \exp(-t/\tau_a)][R_w(t) - R_\infty], \quad (13)$$

in which τ_a is an atmospheric spinup time, reflecting the timescale of response of the atmosphere from its initial state. Using this relation together with the exponential curve to evaluate 30-day R_w, we estimated A_T for all grid points and simulation start dates so as to minimize the squared difference between the two sides of this equation. For this purpose, we also vary τ_a, but we prescribe a maximum value of 2 weeks, which is characteristic of a saturation timescale for atmospheric error growth (cf. Palmer 1993; Simmons et al. 1995; Shukla and Kirtman 1996). Perhaps the most dubious aspects in estimating our A_a metric [i.e., curve fit of Eq. (13)] are for grid points in which $\tau_w < \tau_a$, that is, when the soil moisture predictability timescale is relatively short (typically when $\tau_w \lesssim 1$ week; refer to Fig. 5). This would imply that the soil moisture memory is shorter than (or comparable to) the spinup timescale from the

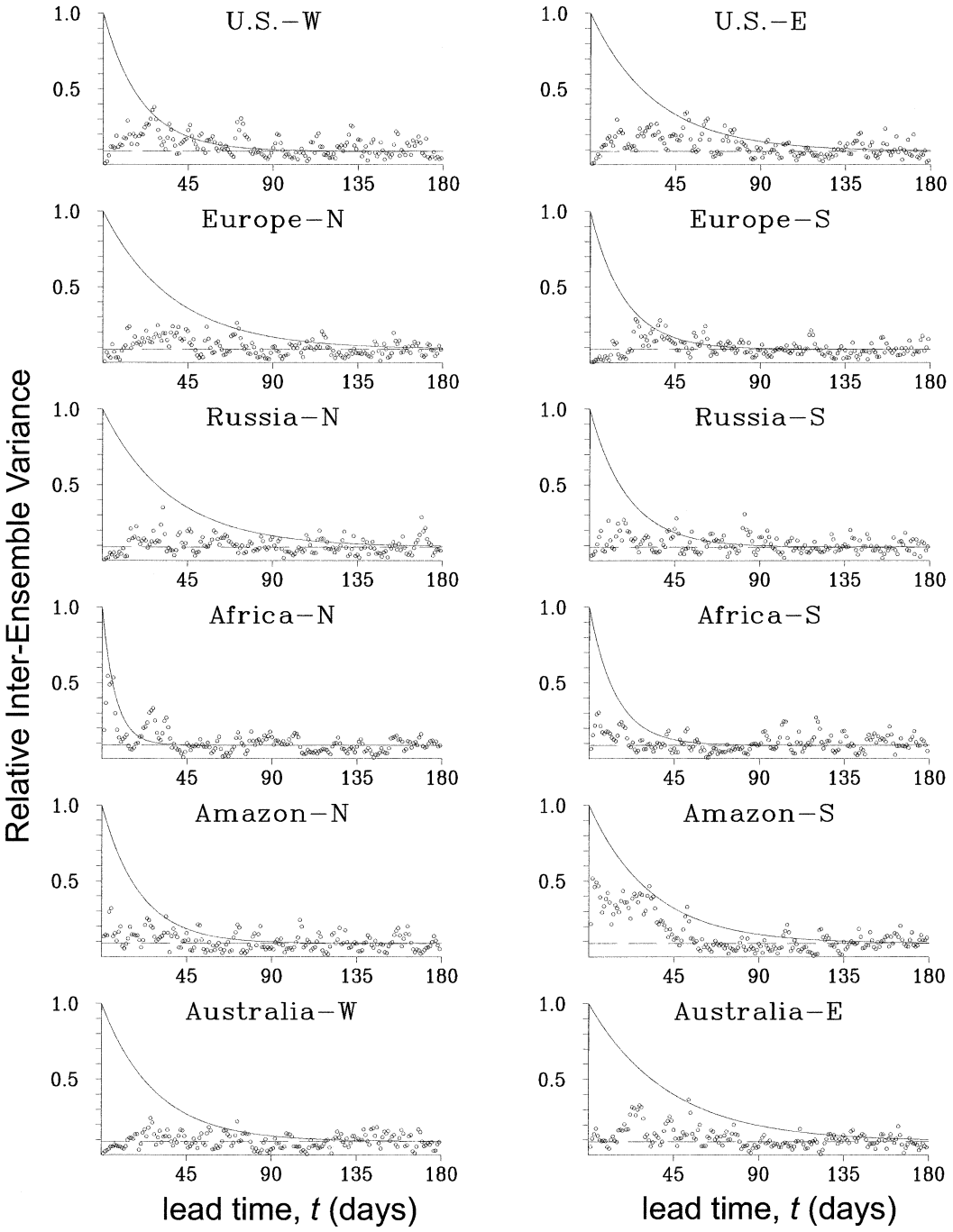

FIG. 6. As in Fig. 2, but for relative interensemble variance of daily near-surface air temperature, R_T, for ensemble simulations starting 1 Jun. Also shown for reference are fitted daily R_w curves (solid lines) and theoretical long lead-time value, R_∞ (dashed horizontal lines).

atmospheric initialization. In such cases, associated atmospheric predictability from soil moisture initialization is intuitively untenable (but from our curve fits result in values close to 1), and we therefore prescribe $A_a = 0$. Figure 8 shows the zonal averages of the fitted curves for the June initialization of the ensemble simulations. Because we use both 30-day R_T and 30-day R_w to solve for A_T in Eq. (13), we distinguish the diagnostic as ''30-day A_T'' (likewise for our precipitation analysis that follows).

Figure 9 shows the dependence of zonal-mean 30-day A_T on latitude and month of initialization. In the

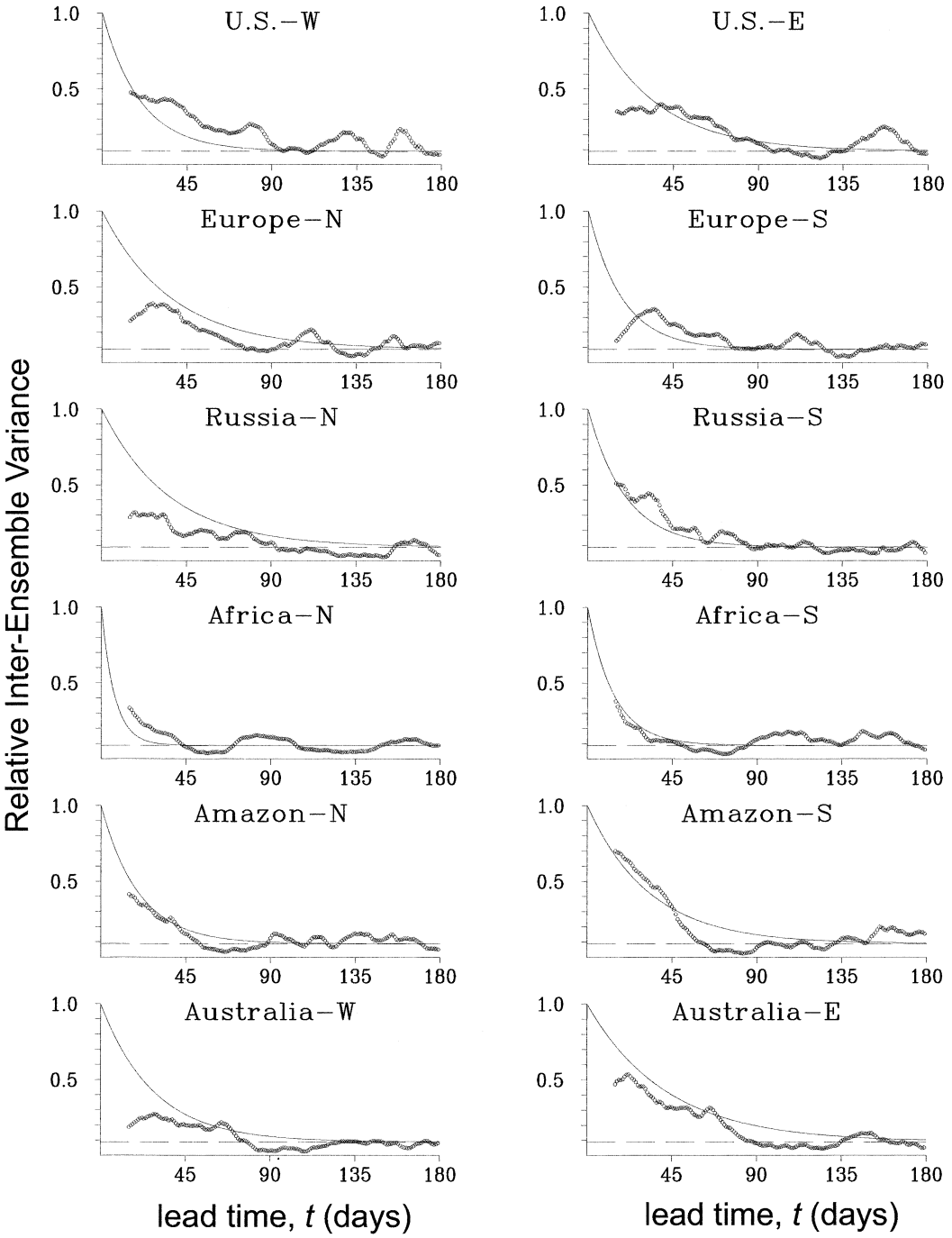

FIG. 7. Relative interensemble variance of 30-day mean near-surface air temperature, 30-day R_T (open circles) for selected grid cells, for ensemble simulations starting 1 Jun, as a function of lead time (days). Also shown are the fitted 30-day R_w curves (solid lines) and the theoretical value of R_∞ (dashed horizontal lines).

Tropics, 30-day A_T is maximized and zonal-mean values are almost always greater than 0.5 and average around 0.75. There is a tendency for the zonal maximum to migrate with the latitude of the intertropical convergence zone. In the northern midlatitudes, 30-day A_T has a strong seasonal cycle, with small values during the cold season and values greater than 0.5 in early summer. The geographical distribution of 30-day A_T is shown in Fig. 10. The global distribution of 30-day A_T is well predicted by the zonal means; there are no strong regional departures from the zonal means.

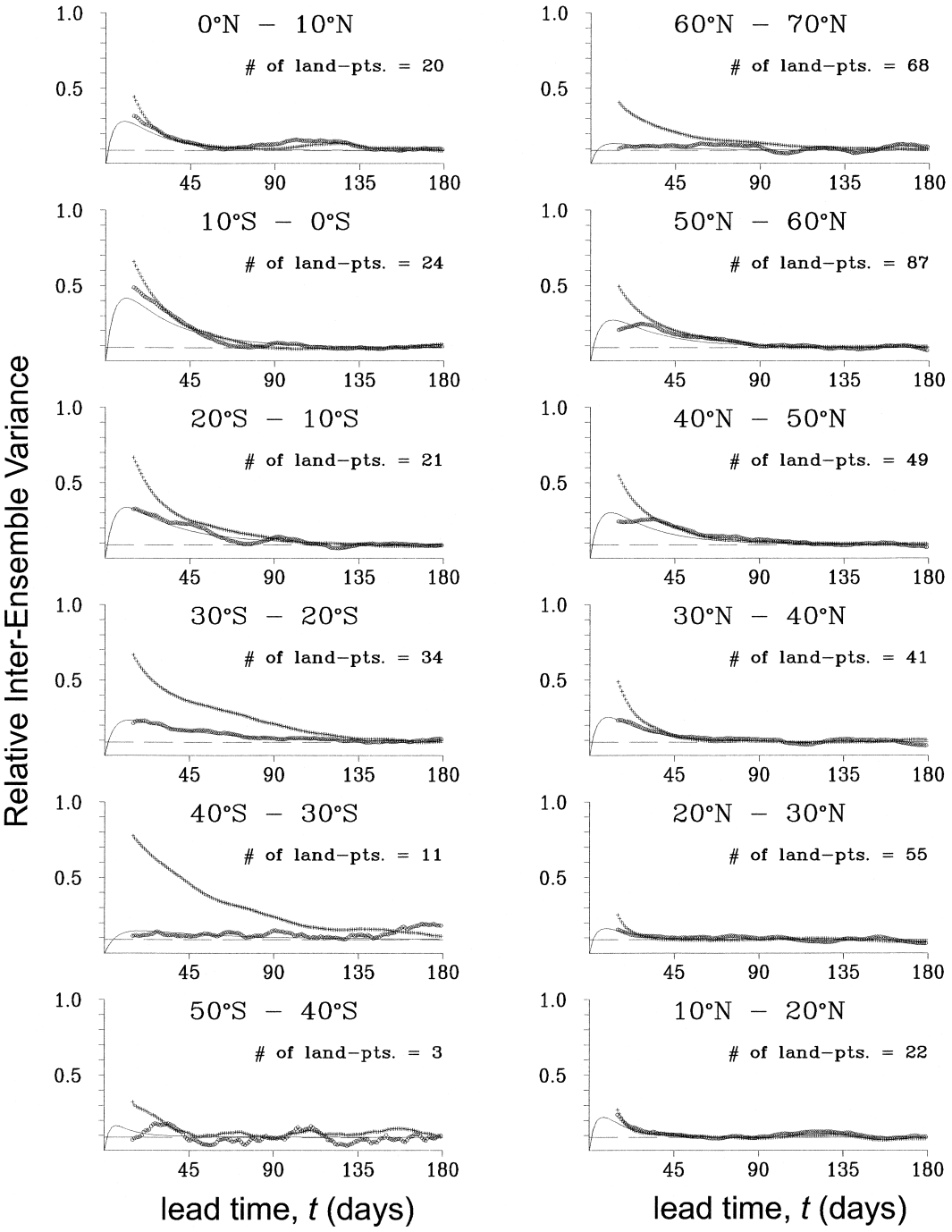

FIG. 8. Zonal averages (land only) of relative interensemble variance for 30-day running mean near-surface air temperature, 30-day R_T (open circle), for ensemble simulations starting in June, as functions of lead time (days). Also shown are the corresponding data for soil moisture, R_w (cross hair), the zonal mean values of the fitted air temperature curve obtained through the curve fit of Eq. (13) (solid line), and the theoretical value of R_∞ (dashed horizontal line).

c. Associated predictability of precipitation

Analysis of our experiments indicated far less associated predictability for precipitation than for air temperature. Figure 11 shows the zonal-mean traces of 30-day R_P for June initialization. There are departures of 30-day R_P above the asymptotic value that appear to be significant in some cases, but the magnitude of the predictability is negligibly small. As a result, the values of 30-day A_P (not shown) that result from the gridpoint curve fitting of (13) reflect an absence of widespread associated predictability of precipitation in the model.

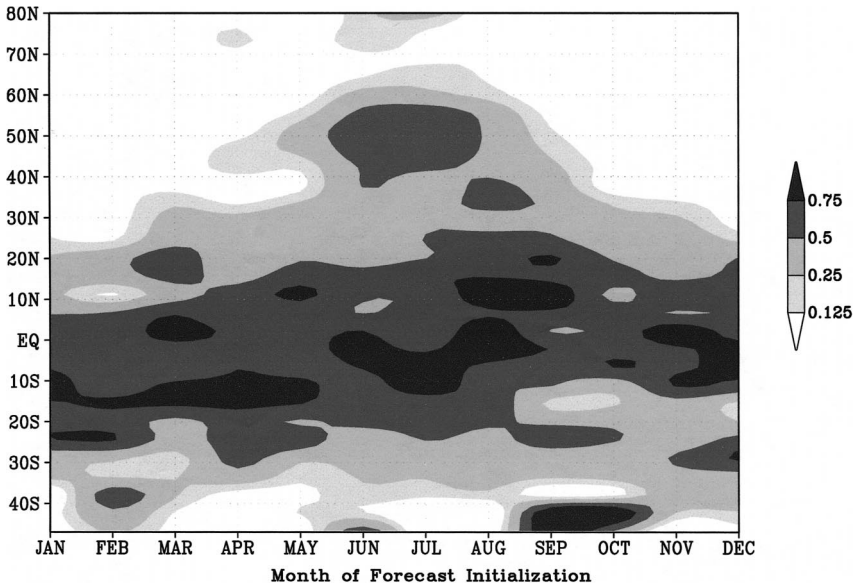

FIG. 9. Zonal-mean values (land only) of 30-day A_T as a function of initialization date of the ensemble simulations and latitude.

The implications of negligible associated precipitation predictability are addressed in the next and concluding sections.

4. Controls of predictability

a. Control of the soil moisture predictability timescale

We have seen empirically that the decay of R_w can be approximated as an exponential function in time. Here we present a theoretical model for the decay. As a starting point, we summarize the model of Delworth and Manabe (1988), which treats soil moisture as a linear, first-order Gauss–Markov process. The soil moisture budget equation (1) can be written as

$$\frac{dw}{dt} = P - \frac{w}{\tau_E} - R, \quad \text{with } w \le w_0, \tag{14}$$

where

$$\tau_E = 0.75 w_0 / E_p. \tag{15}$$

We also assume for now that the soil moisture process is stationary; no seasonality of P or E_p is considered. Delworth and Manabe (1988) have noted that the assumption of uncorrelated, Gaussian ''white noise'' for P, with E_p constant and R negligible, leads to w being a ''red-noise'' process, with an autocorrelation function given by

$$r(t) = \exp(-t/\tau), \tag{16}$$

in which the autocorrelation timescale of soil moisture τ is identical to τ_E. Further, they showed, by simulation of selected cases, that the main effect of runoff is to shorten the timescale, τ, relative to τ_E, under humid climatic conditions (i.e., when mean precipitation is comparable to, or greater than, E_P in magnitude). Although not allowed in the GFDL bucket formulation, runoff can also occur during subsaturated conditions. Thus, w behaves as though (14) and (15) were replaced by

$$\frac{dw}{dt} = P - \frac{w}{\tau}, \tag{17}$$

where $\tau \le \tau_E$.

The soil moisture autocorrelation timescale τ is closely related to the timescale of decay of soil moisture predictability, τ_w, as we show here. Under the assumptions leading to (17), it is possible to describe the growth in variance, σ^2, of w over time after any known initial value (e.g., Gelb 1974, p. 79),

$$\frac{d\sigma^2}{dt} = -\frac{2\sigma^2}{\tau} + q, \tag{18}$$

in which q is the rate of variance production by the process P. In our predictability application, we are interested in the solution of (20) for no initial variance (known initial soil moisture) and P described by a white-noise process (which we assume), which can be written

$$\sigma^2 = (1 - e^{-2t/\tau})\sigma_0^2, \tag{19}$$

where σ_0^2 is the variance of soil moisture for long lead time.

The variance σ^2 is directly related to our soil moisture intraensemble variance (S_A^2), although the former describes a population, whereas the latter is a sample statistic. Likewise, σ_0^2 is a process characteristic and our overall variance (S_T^2) is a sample statistic. Here we ig-

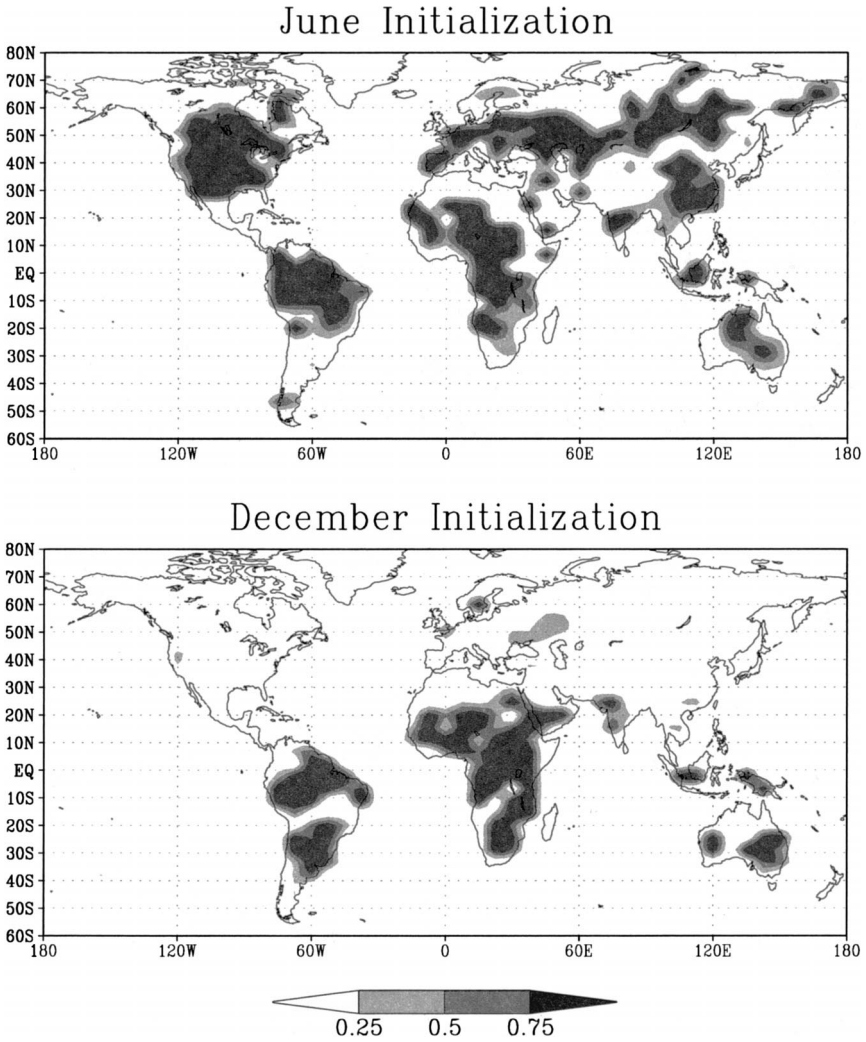

FIG. 10. Global distribution of 30-day A_T for ensemble simulations starting (top) 1 Jun and (bottom) 1 Dec.

nore these distinctions, which is equivalent to assuming that M and N are sufficiently large. Then we find, from (6), (7), and (21),

$$R_w(t) = 1 - \frac{\sigma^2}{\sigma_o^2} = e^{-2t/\tau}. \tag{20}$$

Equation (22) explains the empirically determined exponential character of the R_w curves and predicts their decay timescale to be half the timescale of the decay of soil moisture autocorrelation,

$$\tau_w = \tau/2. \tag{21}$$

All of this theory has been developed without consideration of seasonal changes in climate. To the extent that τ is much shorter than 1 yr, this theory can be assumed to apply during any particular season of the year, with E_p being representative of that season. In seasons for which the τ so determined would be several months or longer, the error of the estimate of τ (and therefore τ_w) will be a function, in part, by antecedent and subsequent statistics of the seasonality of E_p (or, more generally, the atmospheric forcing) as well as the strength of land–atmosphere feedbacks (Koster and Suarez 2001).

In light of these expected limitations, the utility of using (23) to predict τ_w is demonstrated for the simulations initialized in June (Fig. 12). In order to obtain an estimate of τ for (23), 7-day lagged autocorrelations of daily soil moisture are determined from the 200-yr climatological run (described in section 2). These pointwise autocorrelations are then inserted into (16) and solved for τ (with a value of $t = 7$ days). A robust spatial correspondence is found between the predicted and actual values of τ_w, with the global, spatial correlation coefficient significant ($=0.67$, land points only) above the 99% significance level.

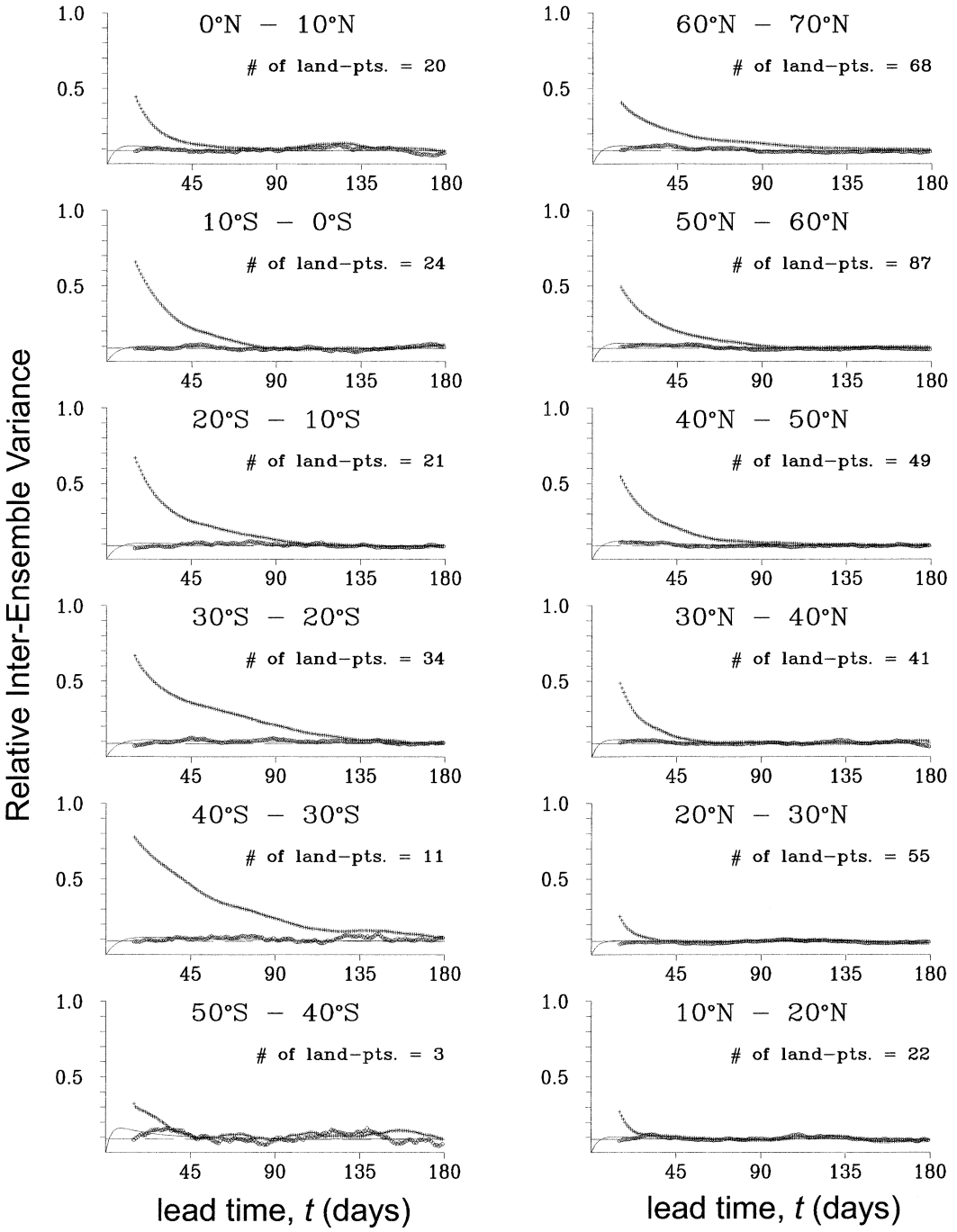

FIG. 11. As in Fig. 8, except for relative interensemble variance of 30-day running mean precipitation, R_P (in place of near-surface air temperature).

b. Control of air temperature predictability

We have introduced A_T as a measure of the translation of soil moisture predictability to predictability of near-surface air temperature. Here we examine the controls of 30-day A_T. We expect significant influence of soil moisture predictability on T predictability when soil moisture variance is a major control of variance in heating of the near-surface environment. Such control can be expected when and where both surface energy availability, R_n (which controls E_p), and the variance of the soil moisture stress factor, β, are large. The simplest index including both these factors is

$$\sigma_\beta \overline{R}_n, \tag{22}$$

in which σ_β is the standard deviation of the monthly

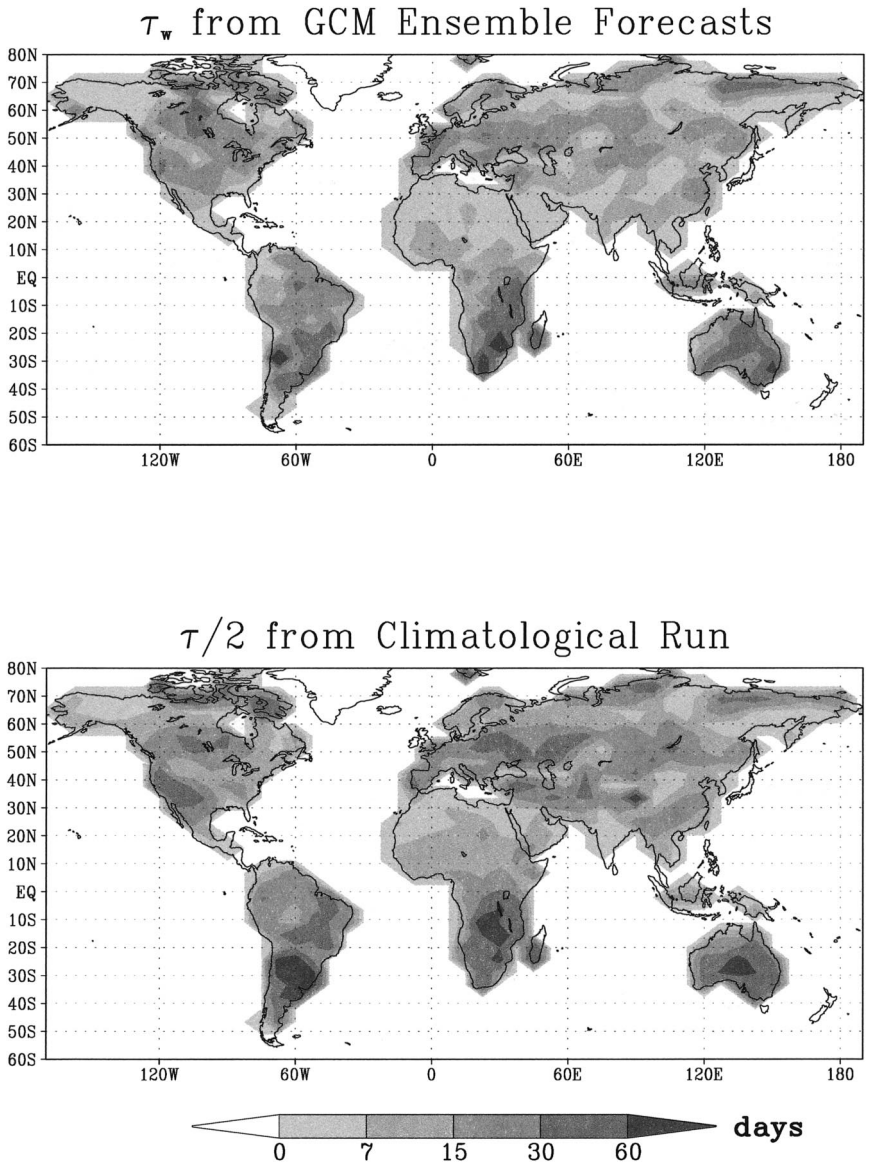

FIG. 12. Global distribution of soil moisture predictability timescales, τ_w. (bottom) Equation (23) is used to obtain a theoretical estimate of τ_w. To obtain an estimate of τ, 7-day lagged autocorrelations from the GCM's 200-yr climatological run are used to solve Eq. (16) with t = 7 days. This estimate is compared to (top) the τ_w values obtained directly from the GCM ensemble simulations. Results are shown for the ensemble simulations initialized 1 Jun.

mean soil moisture stress factor and $\overline{R}_n$ is monthly mean net radiation. Relatively large values of this index should reflect an environment that supports strong, local coupling between soil moisture and turbulent heat-flux partitioning, hence T variability, and, therefore, a high value of 30-day A_T. On the other hand, when (24) is small, we expect 30-day A_T to tend to zero. The ability of this index to predict 30-day A_T is demonstrated for the simulations initialized for June (Fig. 13). The index shows a robust (and significant at the 99% level) consistency with 30-day A_T for June (Fig. 10). Overall, a significant geographical correspondence between this index and 30-day A_T is seen for all initialization months of the ensemble simulations (Fig. 14). However, this correspondence does not necessarily imply causality.

5. Closing remarks

a. Summary

Using a coupled land–atmosphere model, we have explored the nature of soil moisture predictability and associated atmospheric predictability. Sets of ensemble simulations were performed using the GFDL R15 GCM

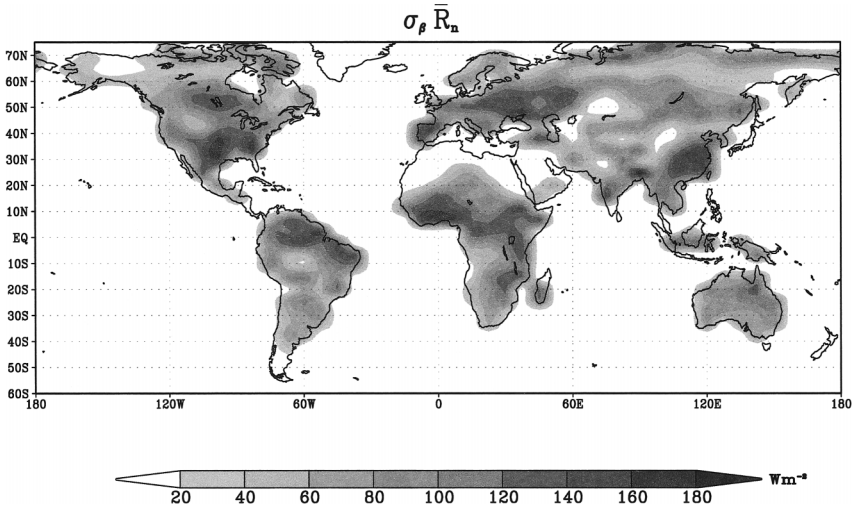

FIG. 13. Global distribution of the product of the variance of the bucket soil moisture stress term, σ_β, and the mean net radiation at the surface, $\overline{R}_n$. Variance and mean are based on Jun mean outputs from the 200-yr climatological run of the GCM.

(forced with climatological SSTs) coupled to a simple land model. A timescale of soil moisture predictability and a measure of the local impact of predicted soil moisture on near-surface air temperature and precipitation predictability are defined in terms of normalized interensemble variance.

The predictability timescale of soil moisture is found to vary from approximately 2 weeks up to 6 months and depends on location (primarily latitude) and the season of initialization. The longest timescales of soil moisture predictability are associated with simulations that start in the winter at mid- and high-latitude regions. The shortest timescales are largely confined to the Tropics and subtropics. However, timescales are also at their shortest at midlatitudes for simulations starting in the summer. The long timescales of soil moisture predictability at high latitudes are likely a result of low potential evaporation rates and the presence of snow cover,

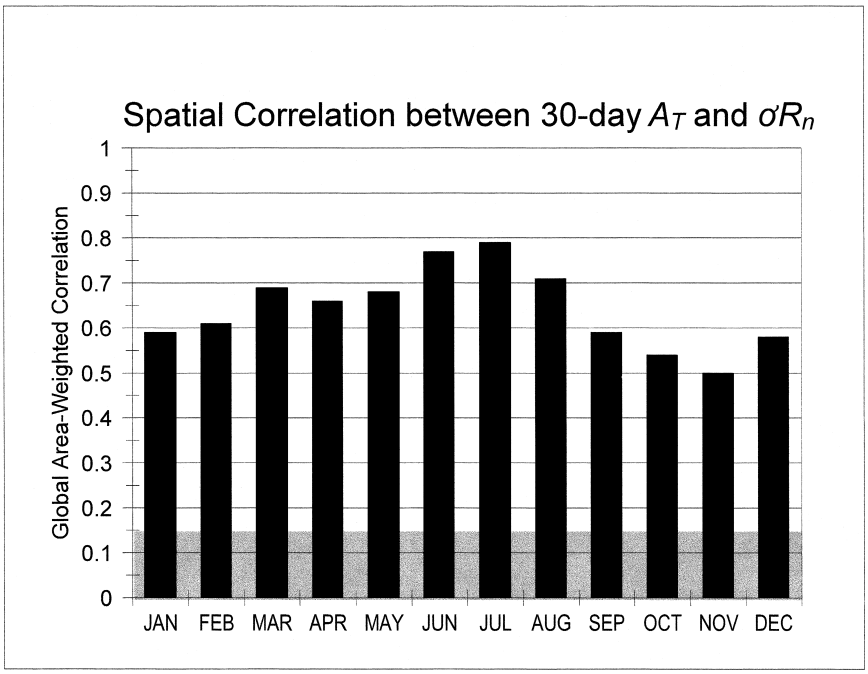

FIG. 14. Monthly results of the spatial (area weighted) correlations between the global fields of σ_β, $\overline{R}_n$, and 30-day A_T. The nonshaded area represents values above the 99% significance level (two-tailed test).

which in the GFDL bucket hydrology decouples soil moisture from the atmosphere.

The associated predictability of near-surface air temperature over the land is strongest in the Tropics and the subtropics. However, a notable impact is also seen in the midlatitudes for simulations initialized in the late spring through summer. The associated predictability of precipitation, however, is insensitive, locally, to predicted soil moisture. The geographic locations of greatest associated predictability of near-surface air temperature are coincident with locations in which net radiation at the surface is abundant and the temporal variability of soil moisture control on surface heat fluxes is high. No substantial associated precipitation predictability of precipitation was found.

b. Discussion

The diagnostic results of simulated soil moisture predictability and associated atmospheric predictability are, indeed, model dependent. This study was based on numerical experimentation using the GFDL AGCM coupled to a simple land model. The theoretical relationship (presented in section 3) between soil moisture persistence and predictability timescales [Eq. (23)] was built upon the GFDL land model's linear relation between soil moisture and its stress on evapotranspiration (among other simplifying assumptions), which allows the soil moisture budget equation to be viewed as a linear Markov process. More complex (i.e., nonlinear) relations between soil moisture and its stress on evapotranspiration exist in most land models that are used for computational climate research [for reviews see Shao and Henderson-Sellers (1996) and Mahfouf et al. 1996)]. As such, the relation between soil moisture predictability and persistence presented in this work is not guaranteed to apply as a general rule. However, a recent study by Koster and Milly (1997) shows that the annual cycle of the water budgets of more complex land models can be captured through linear approximations (as a function of soil moisture) of their evaporation and runoff formulations. Therefore, it is reasonable to expect that, to a certain extent, the relation between soil moisture predictability and persistence in most land models can be approximated through a linear, Markovian framework. Perhaps more compelling, the results of Vinnikov and Yeserkepova (1991) using gravimetric soil moisture observations (for primarily grassland plots) over the former Soviet Union empirically support the Markovian behavior of soil moisture persistence and, therefore, by extension of our analysis, its predictability. Therefore, while the limited scope (both in space and bio-geological extent) of their observations precludes any general conclusions in this regard, it warrants further studies to do so.

A similar consideration of our theory relating soil moisture predictability and persistence should be made with regard to nonlinear and nonlocal interactions between soil moisture and precipitation (as well as a remote SST influence on precipitation, which is addressed in a subsequent paragraph). Note that for the limiting case of a local, linear interaction between soil moisture and precipitation, a linear damping term similar to that used for evapotranspiration stress (i.e., the β term) can be included in the soil moisture budget equation [Eqs. (14) and (17)] to represent the local response of precipitation to soil moisture. Therefore, the essence of the linear Markov process for soil moisture is retained. However, a nonlocal and/or nonlinear impact of soil moisture on precipitation cannot be conveniently described within the context of a linear Markov representation of the soil moisture budget. Nevertheless, any persistence of precipitation induced by nonlinear and/or nonlocal feedbacks will, in turn, enhance soil moisture persistence and predictability [beyond what would be estimated by Eq. (23)]. In this case, our theoretical model of the soil moisture predictability timescale could be viewed as an underestimate. The results of recent numerical experiments (Koster et al. 2002) show a wide range of strength in land–atmosphere coupling (in particular, the response of precipitation to land surface evaporation efficiency) for four particular GCMs. The precipitation processes that are parameterized, the land–atmosphere coupling strategies employed, (Polcher et al. 1998) as well as the degree to which near-surface atmospheric profiles are adequately resolved (K. Findell 2002, personal communication) likely contribute to the model scatter and the accuracy of any model result. These issues further underscore the sensitivity of the numerical representation of coupled-climate processes on their coupled modes of predictability. Nevertheless, the low A_P found in our analysis [qualitatively consistent with three of the four GCMs' results in Koster et al. (2002)] is indicative of a weak, local soil moisture–precipitation interaction in the GFDL GCM. Therefore, our theoretical model [Eq. (23)] is able to predict the soil moisture predictability timescales reasonably well (Fig. 12), because the theory leading to Eq. (23) is based upon an assumption (among others) that precipitation is a white-noise process (i.e., no land–atmosphere feedbacks occur).

Our relation between soil moisture persistence and predictability further emphasizes the crucial role accurate soil moisture modeling plays in climate prediction; if a particular land model exhibits spurious modes of soil moisture persistence (due to inaccurate parameterizations), this will likely lead to spurious modes of soil moisture predictability (and associated atmospheric predictability). As such, future efforts should be made to evaluate simulated soil moisture persistence of current land models over large scales (continental to global) at resolutions consistent with AGCMs. Current efforts to run land models at the global scale over many years (Polcher 2000), as well as the collection of in situ (e.g., Entin et al. 2000) and remote sensing data (e.g., Walker

and Houser 2001) to monitor and analyze soil moisture globally, will prove valuable in this regard.

Delworth and Manabe (1988) showed some redness and, hence, some (implied) associated predictability of spatially filtered (i.e., nine-point smoothed) precipitation in the GFDL AGCM. The results presented here indicate that the local impact of soil moisture variability on subsequent precipitation is weak. The apparent disparity between these findings has been addressed by calculating our R and A_a diagnostics on spatially filtered (i.e., five-point smoothed) soil moisture and precipitation fields. These complementary diagnostics were conducted for the forecasts starting 1 June and indicate that spatially filtered values of precipitation lead to small, but discernible, peaks of 30-day R_P that rise above R_∞ at early lead times (unlike the flat curves of zonally averaged 30-day R_P shown in Fig. 11). This would indicate that spatial filtering of 30-day mean precipitation could lead to more robust results for the A_P diagnostics, but only marginally so. Overall, the results indicate a potential enhancing effect of spatial and temporal averaging on these types of explained-variance/predictability diagnostics.

Looking further at the results of Delworth and Manabe (1989), we see a strong impact of soil moisture variability on the power spectrum of near-surface relative humidity index (a reddening effect). Koster et al. (2000) present an intuitive basis for the conditions in which a strong coupling between land surface and precipitation variability would be expected. They argue (and support through experimental results from their particular GCM) that regions of intermediate near-surface relative humidity (and where the spatial gradients of relative humidity are strong) would be most conducive to a strong land surface–precipitation interaction. The results of this study would indicate that, although a strong coupling between soil moisture and near-surface relative humidity exists in the GFDL GCM, this does not translate into widespread precipitation predictability. This disparity could be a result of the fact that the apparent near-surface humidity control in the GFDL GCM is largely a manifestation of soil moisture's control on near-surface temperature variability (supported by the strong A_T results) rather than a moisture flux effect (via surface evaporation).

These predictability experiments were conducted using climatological SSTs as boundary conditions. Therefore, any influence of ocean variability on these predictability results was removed. In light of the wealth of numerical studies that have studied the impact of the ocean on atmospheric variability and predictability (e.g., see section 1), it is reasonable to assume that including knowledge of interannual SST variations in these experiments would cause an appreciable (and predictable) response of the atmosphere (i.e., a precipitation anomaly). Over the continents, any predictable precipitation response could result in a predictable soil moisture anomaly. While this may lead to enhanced predictability of soil moisture (and the atmosphere), it is the result of an atmospheric response to the ocean, rather than the response to initial soil moisture information. Our intent for these experiments was to obtain the predictability signal that results solely from the knowledge of initial soil moisture, and therefore we have removed the ocean influence.

Nevertheless, the results presented indicate that initial soil moisture information would have a widespread, predictable effect on climate predictions with the GFDL GCM for monthly soil moisture and near-surface air temperature, especially for the Tropics and subtropics, and for forecasts starting in the summer at midlatitudes. Many previous GCM experiments have investigated the impact of soil moisture initialization on simulating extreme climate events (e.g., Atlas et al. 1993) and in some cases used idealized and/or extreme values for their soil moisture initialization (e.g., Oglesby 1991). Studies like these are useful for ascertaining the role of land–atmosphere interactions under extreme conditions but cannot quantify whether these events are predictable, or whether soil moisture can provide a useful predictive impact for climate simulations under less extreme climate conditions. The global soil moisture fields used to initialize the ensemble simulations were essentially taken at random from a climatological run of the GFDL GCM. Therefore, a wide range of soil moisture conditions (i.e., from wet to dry regions) is represented. As such, our analysis reflects a broader perspective of the impact of soil moisture initialization on soil moisture predictability and its subsequent predictable impact in coupled climate simulations.

Acknowledgments. We wish to thank Syukuro Manabe, Tom Delworth, Timothy DelSole, and Jeffery Anderson for valuable discussions and insights during the course of this study. We thank Randy Koster, Paul Dirmeyer, Kirsten Findell, and two anonymous reviewers for constructive and insightful comments. We would also like to thank Krista Dunne for providing her technical expertise during the construction of the numerical experiments. All figures except Fig. 14 were plotted using the GrADS software developed by Brian Doty.

REFERENCES

Atlas, R., N. Wolfson, and J. Terry, 1993: The effect of SST and soil moisture anomalies on GLA model simulations of the 1988 U.S. summer drought. *J. Climate*, **6,** 2034–2048.

Charney, J. G., R. G. Fleagle, H. Riehl, V. E. Lally, and D. Wark, 1966: The feasibility of a global observation and analysis experiment. *Bull. Amer. Meteor. Soc.*, **47,** 200–220.

Delworth, T. D., and S. Manabe, 1988: The influence of potential evaporation on the variabilities of simulated soil wetness and climate, *J. Climate*, **1,** 523–547.

——, and ——, 1989: The influence of soil wetness on near-surface atmospheric variability. *J. Climate*, **2,** 1449–1462.

——, and ——, 1993: Climate variability and land-surface processes. *Adv. Water Res.*, **16,** 3–20.

Dirmeyer, P. A., 1995: Problems in initializing soil wetness. *Bull. Amer. Meteor. Soc.*, **76,** 2234–2240.
——, 1999: Assessing GCM sensitivity to soil wetness using GSWP data. *J. Meteor. Soc. Japan*, **77,** 367–384.
Durre, I., J. M. Wallace, and D. P. Lettenmaier, 2000: Dependence of extreme daily maximum temperatures on antecedent soil moisture in the contiguous United States during summer. *J. Climate*, **13,** 2641–2651.
Entin, J., A. Robock, K. Ya. Vinnikov, S. E. Hollinger, S. Liu, and A. Namkhai, 2000: Temporal and spatial scales of observed soil moisture variations in the extratropics. *J. Geophys. Res.*, **105,** 11 865–11 878.
Fennessy, M., and J. Shukla, 1999: Impact of initial soil wetness on seasonal atmospheric prediction. *J. Climate*, **12,** 3167–3180.
Gelb, A., Ed.,1974: *Applied Optimal Estimation.* MIT Press, 374 pp.
Gordon, H. B., and B. G. Hunt, 1987: Interannual variability of the simulated hydrology in a climatic model—Implications for drought. *Climate Dyn.*, **1,** 113–130.
Houser, P. R., W. J. Shuttleworth, J. S. Famiglietti, H. V. Gupta, K. H. Syed, and D. C. Goodrich, 1998: Integration of soil moisture remote sensing and hydrologic modeling using data assimilation. *Water Resour. Res.*, **34,** 3405–3420.
Huang, J., and H. M. van den Dool, 1993: Monthly precipitation–temperature relations and temperature prediction over the United States. *J. Climate*, **6,** 1350–1362.
Koster, R. D., and M. J. Suarez, 1996: The influence of land surface moisture retention on precipitation statistics. *J. Climate*, **9,** 2551–2567.
——, and P. C. D. Milly, 1997: The interplay between transpiration and runoff formulations in land surface schemes used with atmospheric models. *J. Climate*, **10,** 1578–1591.
——, and M. J. Suarez, 2001: Soil moisture memory in climate models. *J. Hydrometeor.*, **2,** 558–570.
——, ——, and M. Heiser, 2000: Variance and predictability of precipitation at seasonal-to-interannual timescales. *J. Hydrometeor.*, **1,** 26–46.
——, P. A. Dirmeyer, A. N. Hahmann, R. Ijpelaar, L. Tyahla, P. Cox, and M. J. Suarez, 2002: Comparing the degree of land–atmosphere interaction in four atmospheric general circulation models. *J. Hydrometeor.*, **3,** 363–375.
Lau, N.-C., and M. J. Nath, 1990: A general circulation model study of the atmospheric response to extratropical SST anomalies observed in 1950–1979. *J. Climate*, **3,** 965–989.
Lorenz, E. N., 1965: A study of the predictability of a 28-variable atmospheric model. *Tellus*, **17,** 321–333.
Mahfouf, J.-F., and Coauthors, 1996: Analysis of transpiration results from the RICE and PILPS Workshop. *Global Planet. Change*, **13,** 73–88.
Manabe, S., 1969: Climate and ocean circulation. Part I: The atmospheric circulation and the hydrology of the earth's surface. *Mon. Wea. Rev.*, **97,** 739–774.
Milly, P. C. D., and K. Dunne, 1994: Sensitivity of the global water cycle to the water-holding capacity of land. *J. Climate*, **7,** 506–526.
Mitchell, K., and Coauthors, 1999: The collaborative GCIP Land Data Assimilation (LDAS) project and supportive NCEP uncoupled land-surface modeling initiatives. Preprints, *15th Conf. on Hydrology*, Long Beach, CA, Amer. Meteor. Soc., 1–4.
Namias, J., 1963: Surface–atmosphere interactions as fundamental causes of droughts and other climatic fluctuations. *Arid Zone Research*, Vol. 20, *Changes of Climate: Proc. of Rome Symposium*, Rome, Italy, UNESCO, 345–359.
——, 1991: Spring and summer 1988 drought over the contiguous United States—Causes and prediction. *J. Climate*, **4,** 54–65.
Oglesby, R. J., 1991: Springtime soil moisture, natural climate variability, and North American drought as simulated by the NCAR Community Climate Model I. *J. Climate*, **4,** 890–897.
Palmer, T. N., 1993: Extended-range atmospheric prediction and the Lorenz model. *Bull. Amer. Meteor. Soc.*, **74,** 49–65.
Polcher, J., 2000: GLASS implementation underway. *GEWEX News*, **10** (4), 9.
——, and Coauthors, 1998: A proposal for a general interface between land surface schemes and general circulation models. *Global Planet. Change*, **19,** 261–276.
Press, W. R., B. P. Flannery, S. A. Teulosky, and W. T. Vetterling, 1986: *Numerical Recipes: The Art of Scientific Computing.* Cambridge University Press, 702 pp.
Shao, Y., and A. Henderson-Sellers, 1996: Validation of soil moisture simulation in land surface parameterization schemes with HAPEX data. *Global Planet. Change*, **13,** 11–46.
Shukla, J., 1998: Predictability in the midst of chaos: A scientific basis for climate forecasting. *Science*, **282,** 728–731.
——, and B. Kirtman, 1996: Predictability and error growth in a coupled ocean–atmosphere model. COLA Tech. Rep. 24, 11 pp. [Available from Center for Ocean–Land–Atmosphere Studies, Suite 302, 4041 Powder Mill Rd., Calverton, MD 20705.]
Simmons, A. J., R. Mureau, and T. Petroliagis, 1995: Error growth and estimates of predictability from the ECMWF forecasting system. *Quart. J. Roy. Meteor. Soc.*, **121,** 1739–1771.
Smagorinsky, J., 1969: Problems and promises of deterministic extended range forecasting. *Bull. Amer. Meteor. Soc.*, **50,** 286–311.
Stern, W., and K. Miyakoda, 1995: Feasibility of seasonal forecasts inferred from multiple GCM simulations. *J. Climate*, **8,** 1071–1085.
Vinnikov, K. Ya., and I. B. Yeserkepova, 1991: Soil moisture: Empirical data and model results. *J. Climate*, **4,** 66–79.
Walker, J. M., and P. R. Rowntree, 1977: The effect of soil moisture on circulation and rainfall in a tropical model. *Quart. J. Roy. Meteor. Soc.*, **103,** 29–46.
——, and P. R. Houser, 2001: A methodology for initializing soil moisture in a global climate model: Assimilation of near-surface soil moisture observations. *J. Geophys. Res.*, **106,** 11 761–11 774.
Yeh, T.-C., R. T. Wetherald, and S. Manabe, 1984: The effect of soil moisture on short-term climate and hydrology change—A numerical experiment. *Mon. Wea. Rev.*, **112,** 474–490.